Computation of Rates of General Corrosion Using Electrochemical and Thermodynamic Models

*A. Anderko, P. McKenzie, and R.D. Young**

ABSTRACT

A comprehensive model has been developed for simulating the rates of general corrosion of selected metals in aqueous solutions. The model consists of a thermophysical and an electrochemical module. The thermophysical module is used to calculate the speciation of aqueous solutions and to obtain concentrations, activities, and transport properties of individual species. The electrochemical module simulates partial oxidation and reduction processes on the surface of the metal. It is capable of reproducing the active-passive transition and the effect of solution species on passivity. The model has been implemented in a program that can be used to simulate the effects of conditions such as temperature, pressure, pH, component concentrations, and flow velocity on corrosion rates. Application examples are presented for carbon steel in aerated systems in the presence of selected inorganic inhibitors. Good agreement with experimental data was obtained.

KEY WORDS: carbon steel, electrochemical kinetics, inhibitors, modeling, prediction, thermodynamics

INTRODUCTION

Rates of general corrosion in aqueous environments depend on a multitude of factors such as the chemistry of the aqueous solution, concentrations of components, temperature, presence of nonaqueous phases, hydrodynamic conditions, and metallurgical factors. Therefore, it is desirable to rationalize and predict the effects of these factors using computational models. For selected systems, models for calculating rates of corrosion have been developed by various investigators in the form of semi-empirical correlations, electrochemical models, or expert systems.[1–11] In this work, a model is presented that is capable of taking into account the chemistry of the investigated systems in a comprehensive way. The model is designed to provide a realistic representation of chemical equilibria and thermophysical properties in the bulk solution and, at the same time, to account for the phenomena at the metal-solution interface. To achieve this, the model should satisfy the following requirements:

—Utilize a comprehensive thermodynamic model to compute the speciation and activities of species in the aqueous solution;

—Utilize models for calculating transport properties, which are necessary to predict mass-transfer effects;

—Represent the partial cathodic and anodic processes on the metal surface;

—Reproduce the active-passive transition and the effect of active ions on passivity;

—Reproduce experimental corrosion rates using parameters calibrated on the basis of a limited amount of data; and

—Be implemented in an easy-to-use program.

In previous studies, a preliminary version of this model was applied to calculate the rates of corrosion in concentrated bromide brines and carbon dioxide/hydrogen sulfide (CO_2/H_2S) systems.[12-13] In this study, it was applied to simulate the corrosion rates

Submitted for publication January 2000; in revised form, September 2000. Presented as paper no. 479 at CORROSION/2000, March 2000, Orlando, Fl.

* OLI Systems Inc., 108 American Road, Morris Plains, NJ 07950.

0010-9312/01/000041/$5.00+$0.50/0

of carbon steel in aerated aqueous systems in the presence of inhibitors.

THERMOPHYSICAL MODULE

The starting point for corrosion analysis is the computation of speciation in the investigated system. For this purpose, a thermodynamic model of electrolyte systems is used. This model combines information about standard-state properties of all species of interest with a formulation for the excess Gibbs energy, which accounts for solution nonideality. The model has been described in detail by Zemaitis, et al.,[14] and Rafal, et al.[15] Here, its essential elements are summarized in Appendix A.

The thermodynamic model is used to predict the concentrations and activities of ionic and neutral species in multicomponent systems that may contain an aqueous phase, any number of solid phases, and, if necessary, a vapor and a nonaqueous liquid phase. Activities of individual species are further used in the electrochemical model. After completing speciation calculations, the thermophysical module computes several properties of the solution including pH, density, electrical conductivity, viscosity, and diffusivity.

ELECTROCHEMICAL MODULE

The electrochemical model takes into account reactions on the surface of the metal and transport processes for the species that participate in the reactions. The model includes passivation phenomena, which may be influenced by pH and the presence of inhibitors. Further, the model combines the partial processes to compute corrosion rates in the framework of the mixed potential theory.

Anodic Reactions

The mechanism of dissolution of iron has been investigated extensively in acidic solutions.[16] While several variations of this mechanism have been proposed, the dependence of the dissolution rate on the activity of hydroxide ions is generally accepted. The mechanism proposed by Bockris, et al.:[17]

$$Fe + OH^- \rightarrow FeOH_{ads} + e^- \quad (1)$$

$$FeOH_{ads} \rightarrow FeOH^+_{ads} + e^- \quad \text{(rate - determining)} \quad (2)$$

$$FeOH^+_{ads} \rightarrow Fe^{2+} + OH^- \quad (3)$$

predicts that the reaction order with respect to the hydroxide ion is 1, which has been verified experimentally for acidic solutions.[17] Additionally, the current density for iron dissolution has been found to depend on the activity of water.[18] The mechanism of Bockris, et al.,[17] also predicts that the anodic transfer coefficient is equal to 1.5. Thus, the current density for iron dissolution is given by:

$$i_{Fe} = i^0_{Fe} \exp\left[\frac{\alpha_{Fe} F\left(E - E^0_{Fe}\right)}{RT}\right] \quad (4)$$

where i^0_{Fe} is the exchange current density, $\alpha_{Fe} = 1.5$, R is the gas constant, T is temperature, and E^0 is the reversible potential of iron dissolution. In addition to the dependence of the exchange current density on the activity of hydroxide ions, there is ample experimental evidence of a dependence on the activity of water.[18] Therefore, the exchange current density for acidic solutions can be expressed as:

$$i^0_{Fe} = i^*_{Fe} a_{OH^-} a^c_{H_2O} \quad (5)$$

where a denotes activities and c is a reaction order with respect to the activity of water and is equal to 1.6.[18]

Although the reaction order with respect to hydroxide ions is valid for acidic solutions, it has been found that iron dissolution proceeds with little influence of pH for solutions with pH > ≈ 4. Bockris, et al., explained this phenomenon by assuming a certain nonzero reaction order with respect to ferrous ions and considering the hydrolysis of the ferrous ions that result from the dissolution.[17] Alternatively, the change in the reaction order with respect to hydroxide ions can be reproduced by assuming that the exchange current density is proportional to the surface coverage by hydroxide ions. This assumption is consistent with the reaction mechanism (Equation [1]). Therefore, Equation (5) is proposed to be modified as:

$$i^0_{Fe} = i^*_{Fe} \theta_{OH^-} a^c_{H_2O} \quad (6)$$

It was assumed further that θ_{OH} can be expressed using the Langmuir adsorption model. Then, Equation (6) can be rewritten as:

$$i^0_{Fe} = i^*_{Fe} \frac{a_{OH^-}}{1 + K_{OH^-} a_{OH^-}} a^c_{H_2O} \quad (7)$$

It should be noted that Equation (7) reduces to Equation (5) for low activities of hydroxide (i.e., for acidic solutions). For higher concentrations of hydroxide ions, the reaction order with respect to hydroxide becomes zero.

The reversible potential is calculated from the Nernst equation and depends on the activity of ferrous ions. Additionally, a relationship is utilized that exists between the reversible potential and the exchange current density for anodic dissolution:[3,19]

$$\frac{RT}{\alpha_{Fe}F}\ln\frac{i^0_{Fe}}{i^{0\,\prime}_{Fe}} = E^0_{Fe} - E^{0\,\prime}_{Fe} \quad (8)$$

Equation (8) is applicable in the active range of iron dissolution. It makes it possible to compute the exchange current density for any concentration of ferrous ions once it is established for a given ferrous concentration. Thus, the anodic current density can be calculated from a combination of Equations (4), (7), and (8).

The proposed model for the anodic dissolution of iron represents a balance between physical realism and mathematical simplicity. The requirement of mathematical simplicity is important because the model contains parameters that have to be calibrated on the basis of limited experimental data. Thus, it is important to limit the number of model parameters. More accurate, detailed models that have been developed on the basis of impedance results necessarily contain a large number of parameters.[20] The simplified model proposed in this paper captures the essential characteristics of iron dissolution (in particular, the reaction orders with respect to hydroxide ions and water and their change with pH) and, therefore, is sufficient for developing a semi-empirical computational system.

Cathodic Reactions

In general, cathodic processes may be caused by the reduction of hydrogen ions or water molecules unless additional reducible species (such as oxygen) are present in the solution. In acidic solutions, the reduction of hydrogen is the dominant cathodic reaction:

$$H^+ + e^- \rightarrow 0.5\ H_2 \quad (9)$$

It is generally accepted that the hydrogen reduction reaction may proceed under activation or mass-transfer control.[21] According to basic electrochemical kinetics, the current density for hydrogen reduction can be written as:[21]

$$\frac{1}{i_{H^+}} = \frac{1}{i_{H^+,a}} + \frac{1}{i_{H^+,lim}} \quad (10)$$

where $i_{H^+,a}$ and $i_{H^+,lim}$ are the activation and limiting current densities, respectively. The activation current density for proton reduction is:

$$i_{H^+,a} = i^0_{H^+}\exp\left[\frac{-\alpha_H F\left(E - E^0_H\right)}{RT}\right] \quad (11)$$

where $\alpha_H = 0.5$[17] and E^0_H is calculated from the Nernst equation using the previously calculated activities of hydrogen ions and elemental hydrogen. To calculate the exchange current density, an expression is introduced that relates the exchange current density to the activities of protons and water molecules:

$$i^0_{H^+} = i^*_{H^+}a^{0.5}_{H^+}a^{1.4}_{H_2O} \quad (12)$$

In Equation (12), the reaction orders with respect to the activities of hydrogen and H_2O have been obtained from the studies of Bockris, et al.,[17] and determined from experimental data,[18] respectively.

The limiting current density in Equation (10) results from diffusion-limited transport of protons to the metal surface and can be calculated as:

$$i_{H^+,lim} = k_m F a_{H^+} \quad (13)$$

where k_m is the mass-transfer coefficient. The value of k_m can be calculated if the flow regime, diffusion coefficient of hydrogen ions, and solution viscosity are known. Formulas for the computation of k_m are discussed in Appendix B.

As the pH of a solution increases, the importance of the proton reduction reaction rapidly decreases. In neutral and alkaline solutions, the predominant reaction is the reduction of water molecules:

$$H_2O + e^- \rightarrow 0.5\ H_2 + OH^- \quad (14)$$

Unlike the reduction of protons, the water reduction does not exhibit a limiting current density because there are no diffusion limitations for the transport of H_2O molecules to the surface. Thus, the current density can be expressed as:

$$i_{H_2O} = i^0_{H_2O}\exp\left[\frac{-\alpha_{H_2O}F\left(E - E^0_H\right)}{RT}\right] \quad (15)$$

As in the case of proton reduction, $\alpha_{H_2O} = 0.5$. The reversible potential in Equation (15) is the same as in Equation (11) because the reduction of water is thermodynamically equivalent to the reduction of protons. The reaction order with respect to water activity can be assumed to be the same as that for proton reduction. Thus, the exchange current density is given by:

$$i^0_{H_2O} = i^*_{H_2O}a^{-0.5}_{H}a^{1.4}_{H_2O} \quad (16)$$

In the presence of oxygen, the reduction of dissolved O_2 becomes an important cathodic reaction:

$$O_2 + 4H^+ + 4e^- \rightarrow 2H_2O \quad (17)$$

The oxygen reduction process is subject to mass-transfer limitations because of the diffusion of dis-

solved oxygen molecules. Thus, the expression for the current density for oxygen reduction is analogous to that for hydrogen reduction:

$$\frac{1}{i_{O_2}} = \frac{1}{i_{O_2,a}} + \frac{1}{i_{O_2,lim}} \quad (18)$$

$$i_{O_2,a} = i^*_{O_2} a_{O_2} a_{H^+}^{-0.5} \exp\left[\frac{-\alpha_{O_2} F\left(E - E^0_{O_2}\right)}{RT}\right] \quad (19)$$

$$i_{O_2,lim} = 4 k_m F a_{O_2} \quad (20)$$

Since the reversible potential of oxygen reduction is significantly higher than that of the remaining reactions, the reaction proceeds predominantly under mass-transfer control, and the contribution of Equation (20) is more significant than that of Equation (19). The reversible potential is calculated from the Nernst equation using the thermodynamic properties obtained from the thermodynamic model (Appendix A), and the mass-transfer coefficient is computed as described in Appendix B.

In addition to the reduction of protons, water, and oxygen molecules, the model takes into account the reduction of other solutes that may have oxidizing properties. In particular, the model will be applied in this study to simulate the effect of chromate and nitrite inhibitors. These inhibitors undergo reduction reactions on the metal surface:

$$CrO_4^{2-} + 5H^+ + 3e^- \rightarrow Cr(OH)_3 + H_2O \quad (21)$$

$$NO_2^- + (x+1)H^+ + xe^- \rightarrow \left(\frac{1}{x}\right)N_xO + \left(\frac{x+1}{2}\right)H_2O \quad (22)$$

The expressions for the current density of these reactions have been assumed to be analogous to Equations (18) through (20). That is, the activation contribution to the current density is proportional to the activity of the oxidizing ions, and the mass-transfer limitation is taken into account. The model also incorporates a reaction of water oxidation (i.e., the reverse of Reaction [17]). This reaction becomes significant only at very high values of the potential and, therefore, does not contribute to ordinary corrosion processes.

For all partial processes, the concentration-independent part of the exchange current density (i^*) is assumed to be temperature-dependent by introducing a nonzero enthalpy of activation:

$$i^*(T) = i^*(T_{ref}) \exp\left[-\frac{\Delta H}{R}\left(\frac{1}{T} - \frac{1}{T_{ref}}\right)\right] \quad (23)$$

Kinetics of the partial anodic and cathodic reactions are influenced by the adsorption of solution species (e.g., halide ions) on the surface. In particular, adsorption in concentrated halide solutions may lead to a change in dissolution mechanism and halide-accelerated dissolution. A method for incorporating adsorption phenomena into the electrochemical model has been described in a previous study[13] and will not be discussed here.

Active-Passive Transition

To introduce the active-passive transition into the electrochemical model, a method was used that was originally proposed by Ebersbach, et al.[22] According to this approach, the current that leads to the formation of a passive layer is considered separately from the current that leads to active dissolution. At any instant, a certain fraction of the surface θ_p is assumed to be covered by the passive layer. The change of the passive layer coverage fraction with time can be expressed as:

$$\left(\frac{\partial \theta_P}{\partial t}\right)_{E,a_i} = c i_2 (1 - \theta_P) - K\theta_P \quad (24)$$

where i_2 is the current density that contributes to the formation of a passive layer. The second term on the right-hand side of Equation (24) represents the rate of dissolution of the passive layer, which is proportional to the coverage fraction. The parameters c and K are proportionality constants. The total current density is expressed as:

$$i_{Fe,TOT} = \left(i'_{Fe} + i_2\right)(1 - \theta_P) \quad (25)$$

where i'_{Fe} is the current density for active dissolution of iron. Equation (25) can be solved with respect to θ_p, and the result can be substituted into Equation (24). In the stationary state ($t \rightarrow \infty$), the total anodic current becomes:

$$i_{Fe,TOT} = \frac{i'_{Fe} + i_2}{1 + \frac{c i_2}{K}} = \frac{i'_{Fe} + i_2}{1 + \frac{i_2}{i_P}} \quad (26)$$

In Equation (26), the ratio c/K constitutes the passive current density. The current density i_2 can be represented by the usual expression for processes under activation control:

$$i_2 = i_2^0 \exp\left(\frac{\alpha_2 F(E - E_F)}{RT}\right) \quad (27)$$

Thus, in addition to the passive current density, the model of the active-passive transition is character-

ized by two parameters, i_2^0 and α_2. These parameters are determined based on observable characteristics of the active-passive transition such as the Flade potential and the critical current density.[21,23-26]

At present, the model does not take into account the effects of formation of corrosion products such as iron hydroxide gels or other products with ill-defined structure.

Effect of Solution Chemistry on Passivity

In the absence of active ions, the passive current density depends primarily on the pH of the solution.[21] Halide and other active ions cause the breakdown of passive films, which manifests itself in an increase in the passive current in addition to the onset of localized corrosion. However, corrosion inhibitors such as molybdates or chromates may repair passive films, thus reducing the passive current density. In this study, only the effect of solution species on the magnitude of the passive current density was examined, not localized corrosion.

As shown by Vetter, the pH dependence of the corrosion current density in the passive state is determined by a reaction between oxygen ions in the passive oxide layer and protons from the solution.[21] In acidic solution, this dissolution reaction can be written as:

$$\equiv FeO_a(OH)_b + sH^+ = Fe(OH)_g^{t+} \qquad (28)$$

where the symbol "≡" denotes the solid substrate and the formula $\equiv FeO_a(OH)_b$ represents the stoichiometry of the hydrated oxide in the passive layer. In general, the hydrated oxide is subject to compositional variations and the stoichiometry of Reaction (28) may vary. Reaction (28) leads to a negative linear dependence of the logarithm of the passive current density on pH, which is in agreement with experimental data in acidic solutions.[27] For neutral and alkaline solutions, Reaction (28) can be modified as:

$$\equiv FeO_a(OH)_b + uH_2O = Fe(OH)_3^0 \qquad (29)$$

By combining Reactions (28) and (29), an expression can be written for the passive current density as a function of proton and water activity:

$$i_p = k_H a_{H^+}^s + k_{H_2O} a_{H_2O}^u \qquad (30)$$

Equation (30) predicts a linear pH dependence of $\log(i_p)$ in acidic solutions and a pH-independent value for nearly neutral or alkaline solutions. This behavior agrees with experimental results, which show negative linearity to pH ≈ 4 and pH independence thereafter.

To analyze the effect of active ions on the passive current density, an approach was used that has been developed for studying the chemical dissolution kinetics of oxides in aqueous media.[28] In this work, this approach was adapted to the dissolution of passive layers. To develop a mathematical relationship between the activities of aggressive or inhibitive ions and the passive current density, surface reactions between the passive oxide layer and the i-th ion from the solution were considered:

$$\equiv FeO_aOH_b + c_iX_i = \equiv FeO_{di}(OH)_{fi}X_{ci} + e_iOH^- \qquad (31)$$

In Equation (31), the stoichiometry is usually difficult to define because of the dynamic nature of the system and may be, in general, fractional. It is reasonable to assume that Equation (31) is in quasi-equilibrium.[28] Therefore, it may be characterized by an equilibrium constant:

$$K_i = \frac{N_i a_{OH^-}^{e_i}}{\left(N_0 - \sum_k N_k\right) a_{X_i}^{c_i}} \qquad i = 1,\ldots n \qquad (32)$$

where the subscript i pertains to the i-th active ion, N_i is the number of sites per surface unit that are occupied by complexes containing the i-th active ion, and N_0 is the total number of sites per surface area. Equation (32) describes a system of equations that represent surface reactions involving any number of active species. This system may be solved with respect to N_i:

$$N_i = \frac{N_0 K_i \dfrac{a_{X_i}^{c_i}}{a_{OH^-}^{e_i}}}{1 + \sum_k K_k \dfrac{a_{X_k}^{c_k}}{a_{OH^-}^{e_k}}} \qquad (33)$$

The surface reaction (Reaction [33]) is followed by a dissolution reaction. The surface species that forms as a result of Reaction (31) may undergo dissolution reactions that are analogous to Reactions (28) or (29):

$$\equiv FeO_{di}(OH)_{fi}X_{ci} + sH^+ \rightarrow Fe(OH)_g^{f+} + c_iX_i \qquad (34)$$

and

$$\equiv FeO_{di}(OH)_{fi}X_{ci} + uH_2O \rightarrow Fe(OH)_3^0 + c_iX_i \qquad (35)$$

On the right-hand side of Equations (34) or (35), the active anions may further form aqueous complexes with the hydrolyzed iron cations.

In acidic solutions, the dissolution rate for the sites occupied by complexes with active ions is given, according to Equation (34), by:

$$i_{p,i} = k_i N_i a_{H^+}^s \quad (36)$$

whereas the dissolution rate for the free sites is:

$$i_{p,0} = k'_H \left(N_0 - \sum_k N_k \right) a_{H^+}^s \quad (37)$$

The total current density in the passive state is the sum of Equations (36) and (37):

$$i_p = i_{p,0} + \sum_k i_{p,k} \quad (38)$$

Analogous expressions can be written for the active species-assisted dissolution in neutral and alkaline solutions (Equation [36]). Assuming that the surface reactions (Equation [31]) are characterized by the same parameters over the whole pH range, the total passive current density can be expressed as:

$$i_p = \left(k_H a_{H^+}^s + k_{H_2O} a_{H_2O}^u \right) \frac{1 + \sum_i l_i \frac{a_{X_i}^{c_i}}{a_{OH^-}^{e_i}}}{1 + \sum_i K_i \frac{a_{X_i}^{c_i}}{a_{OH^-}^{e_i}}} \quad (39)$$

where l_i is a composite parameter that contains the forward dissolution rate constant (k_i) and the quasi-equilibrium constant K_i. In Equation (39), the k_H and k_{H_2O} parameters are determined using data for passive film dissolution in the absence of active ions.[21,24-25,27,29-32] In the case of halide ions or other species that cause the breakdown of passivity, the l_i parameters are numerically greater than the K_i parameters, which results in a significant increase in the passive current density. This reflects the fact that the surface reaction is followed by accelerated dissolution. However, inhibitor ions are characterized by large K_i and small l_i parameters. Thus, according to the model, inhibitor ions are envisaged to form surface complexes that block the reaction sites on the surface of the passive layer. In this case, the surface reaction is not followed by accelerated dissolution. Thus, the presence of inhibitor ions counteracts the effect of halide ions and limits the current density. In this way, the model simultaneously takes into account the ions that promote the dissolution of the passive film ($K_i < l_i$) and those that inhibit the dissolution ($K_i >> l_i$).

Implementation of the Model

Parameters of the electrochemical model have been determined by utilizing a large number of experimental polarization and corrosion rate data. In particular, parameters for the proton reduction, water reduction, oxygen reduction, and iron oxidation processes were determined from relevant data on the corrosion of iron and mild steel in various mineral acids, bases, and saline solutions.[33-34] The parameters that represent the effect of several inhibiting ions have been calibrated using polarization data[35-37] or experimental corrosion rate data that relate the corrosion inhibition to the solution concentration.[37] Since the model contains empirical parameters obtained from experimental data, the quality of model predictions depends on the data on which the parameters are based. This is a common feature of all semi-empirical models.

Partial electrochemical processes described above are combined into a total predicted polarization curve. The corrosion potential is calculated by applying the mixed-potential theory:

$$\sum i_{c,i} = \sum i_{a,j} \quad (40)$$

where $i_{c,i}$ and $i_{a,j}$ denote the i-th cathodic and j-th anodic process. Once the corrosion potential is obtained by solving Equation (40), the corrosion current density also is computed.

The model has been implemented in a Windows†-based program called the CorrosionAnalyzer†. This program can be used to calculate general corrosion rates once temperature, pressure, and overall concentrations of aqueous stream components are defined. The program performs calculations in two steps. It calculates the speciation and thermodynamic properties (Appendix A). At the end of the speciation calculations, it also computes the transport properties that are necessary for modeling mass-transfer effects. Then, the program uses the previously obtained speciation and transport properties to calculate the partial anodic and cathodic processes that are possible in the system. Finally, the partial electrochemical processes are combined and the corrosion rate and potential are calculated using the mixed potential theory.

APPLICATIONS OF THE MODEL

In previous studies, the electrochemical model was applied to the simulation of corrosion of carbon steel in CO_2/H_2S systems[12] and concentrated bromide brines.[13] In this work, it was applied to study the effect of various inhibitors on the corrosion rate of carbon steels in aerated aqueous solutions.

The presence of inhibitors influences the passive current density as shown by Equation (39). A substantial decrease in the passive current density may give rise to passive behavior and a substantial reduction in corrosion rates. Equation (39) predicts that the passive current density is a strong function of the inhibitor concentration. To verify the performance of

† Trade name.

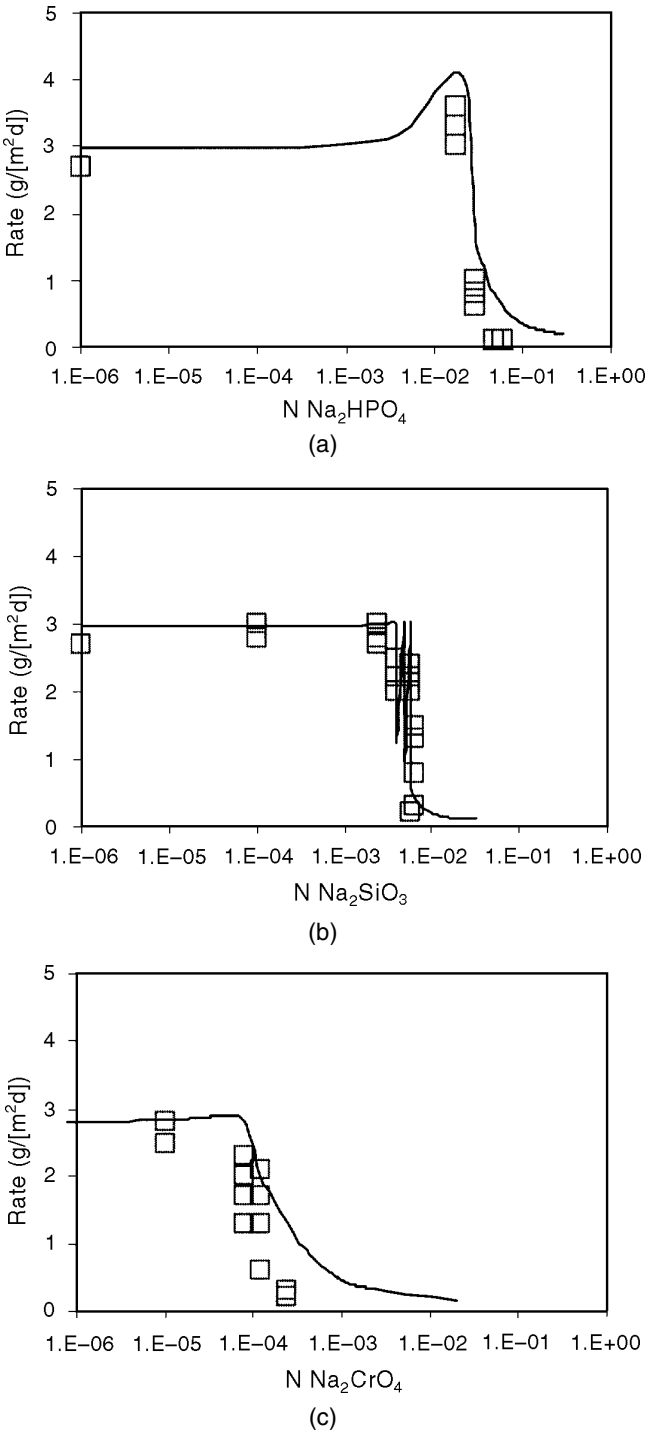

FIGURE 1. *Effect of monobasic phosphate, silicate, and chromate ions on the corrosion rate of carbon steel in aerated water at 25°C. The lines were calculated from the model, and the symbols denote the data of Pryor and Cohen.[38]*

the model, corrosion rates were calculated for carbon steel in aerated water in the presence of several inhibitors. Figure 1 shows the dependence of the calculated corrosion rate on the concentration of three inhibitors (monobasic phosphate, silicate, and chromate ions). In all cases, a fairly sharp transition to passive behavior was observed as the concentration of the inhibitor exceeded a certain threshold value. This threshold value was very low for chromates and substantially higher for monobasic phosphates and silicates. It is noteworthy that the model represents the experimental corrosion rates with very good accuracy.[37]

To examine how this behavior is reproduced by the model, Figure 2 shows the calculated current density vs potential relationships for three concentrations of silicate ions (0, 0.0014, and 0.008 m). Figure 2 includes the partial cathodic and anodic processes that were taken into account for the analysis. The dominant cathodic process was the reduction of oxygen. This process, denoted by "B" in the figure, proceeded under mass-transfer control as shown by the vertical portion of the oxygen reduction line. The iron oxidation process exhibited an active-passive transition, which was strongly influenced by the presence of inhibitors. Without silicate ions (Figure 2[a]), the oxygen reduction line intersected the iron oxidation line in the range of active dissolution of iron. Correspondingly, the corrosion potential was low and the corrosion rate was substantial. With a substantial concentration of silicate ions (Figure 2[c]), the passive current density and critical current density were substantially reduced. Subsequently, the oxygen reduction line intersected the iron oxidation line within the passive range. The corrosion potential increased substantially and the corrosion rate was reduced. For intermediate concentrations of silicate ions (Figure 2[b]), the shape of the predicted iron oxidation line was such that three mixed potentials were possible. This resulted in multiple steady states, and the system oscillated between corrosion in the active and passive states. This is reflected in Figure 1 by several vertical portions of the calculated line, which correspond to the range of predicted corrosion rates for given conditions. Although this behavior cannot be unequivocally corroborated, it is consistent with experimental data in the intermediate concentration range that corresponds to the active-passive transition.

After verifying the predictions for inhibitors in pure aerated water, the model was applied to more complex systems. Figure 3 shows the dependence of the corrosion rate of carbon steel in simulated cooling water as a function of pH and the amount of added nitrate ions. Simulated cooling water contains small, but not negligible, concentrations of chloride and sulfate ions, which contribute to the breakdown of passive films. Thus, the chloride and sulfate ions counteract the effect of the inhibitor ions. The competing effect of various ions is taken into account by Equation (39) for the passive current density. As shown in Figure 3, the corrosion rate is strongly affected by pH. This was caused by the effect of pH on the passive current density (Equation [39]) and

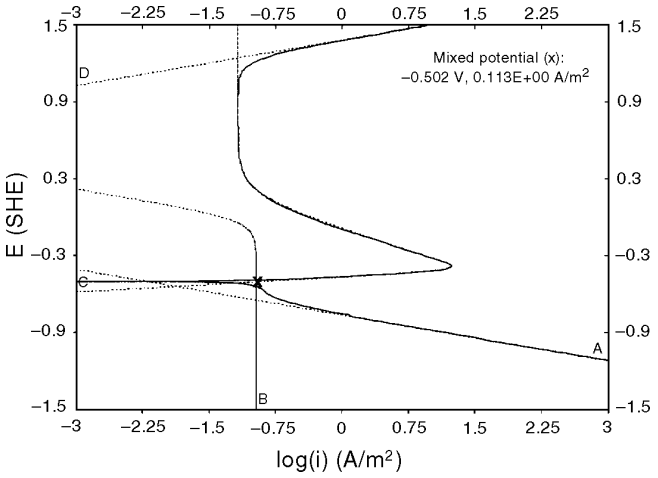

(a)

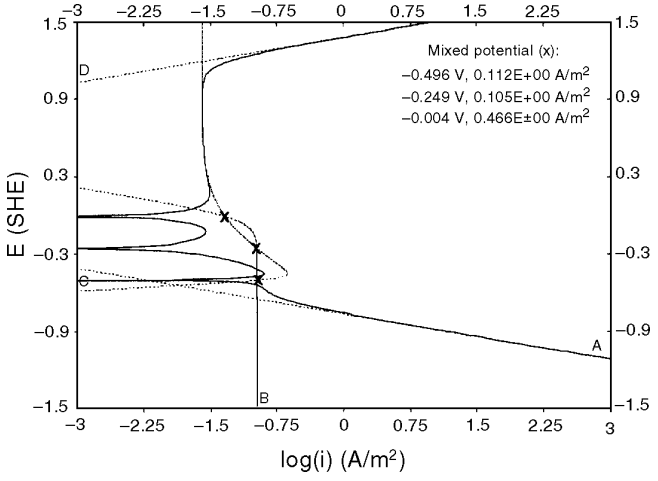

(b)

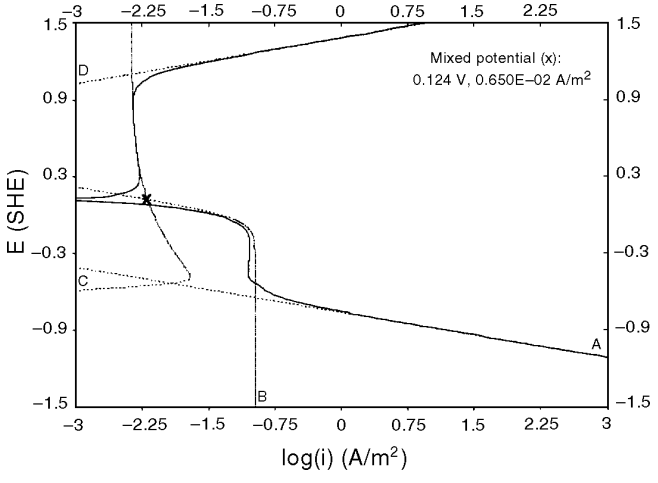

(c)

FIGURE 2. *Predicted current density-potential relationships, including partial anodic and cathodic processes, for carbon steel in aerated water with: (a) no Na_2SiO_3, (b) 0.0014 m Na_2SiO_3, and (c) 0.008 m Na_2SiO_3. The partial processes are denoted by A through D, where A: $H_2O = 0.5\ H_2 + OH^- - e^-$, B: $O_2 + 4H^+ = 2H_2O - 4e^-$, C: $Fe = Fe^{2+} + 2e^-$, and D: $2H_2O = O_2 + 4H^+ + 4e^-$.*

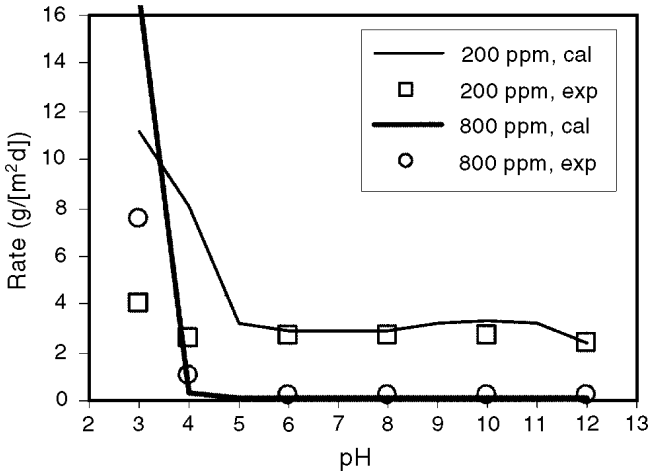

FIGURE 3. *Corrosion rates of carbon steel in simulated cooling water (7×10^{-3} m NaCl, 5.4×10^{-3} m Na_2SO_4, 6.25×10^{-4} $CaCO_3$, and 6.25×10^{-4} m $MgCO_3$) as a function of pH and the concentration of added nitrite ions. The lines were obtained from the model, and the symbols denote the data of Mustafa and Dulal.[39]*

the contribution of the proton reduction reaction (Equation [9]), which becomes significant at lower pH values. As shown in Figure 3, the effect of pH and nitrite concentration is accurately reproduced by the model.

The electrochemical model is particularly suitable for studying the effects of mixtures of inhibitors. This is shown in Figure 4 for the corrosion rate of carbon steel in simulated cooling water in the presence of a mixed molybdate + nitrite inhibitor. Parameters of the electrochemical model were adjusted based on limited experimental data for systems with a single inhibitor.[37-38] With such parameters, the model can be used to make predictions for mixed systems. As shown in Figure 4, the model correctly predicted the pH dependence of corrosion rates in the mixed-inhibitor system.

It is particularly interesting to apply the model to study the synergism of inhibitors with dissolved oxygen. Figure 5 shows results of calculations for carbon steel in simulated cooling water inhibited with a mixture of sodium nitrite ($NaNO_2$) and sodium molybdate (Na_2MoO_4) with varying composition. The total amount of inhibitor ($NaNO_2$ + Na_2MoO_4) is 500 mg/L, and the amount of dissolved oxygen is 1, 2.5, or 5 mg/L. The corrosion rate for the system inhibited with only $NaNO_2$ (i.e., for 0 mg MoO_4) did not depend on the concentration of oxygen. This was caused by the fact that nitrate ions have oxidizing properties (Equation [22]) and contribute to increasing the corrosion potential. However, molybdate ions are not oxidizing and their effect is limited to reducing the passive current density (Equation [39]). However, the reduction of the passive current density was not sufficient, in this case, to achieve passive behavior. Therefore, the corrosion rate of the system inhib-

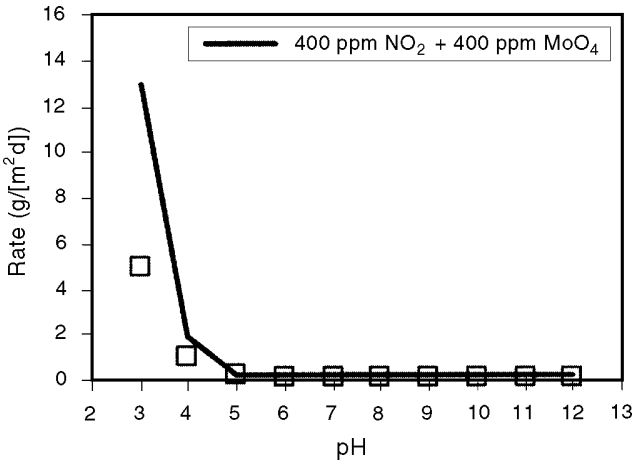

FIGURE 4. *Corrosion rates of carbon steel in simulated cooling water (7×10^{-3} m NaCl, 5.4×10^{-3} m Na_2SO_4, 6.25×10^{-4} $CaCO_3$, and 6.25×10^{-4} m $MgCO_3$) as a function of pH in the presence of 400 ppm of molybdate ions and 400 ppm of nitrite ions. The lines were obtained from the model, and symbols denote the data of Mustafa and Dulal.[39]*

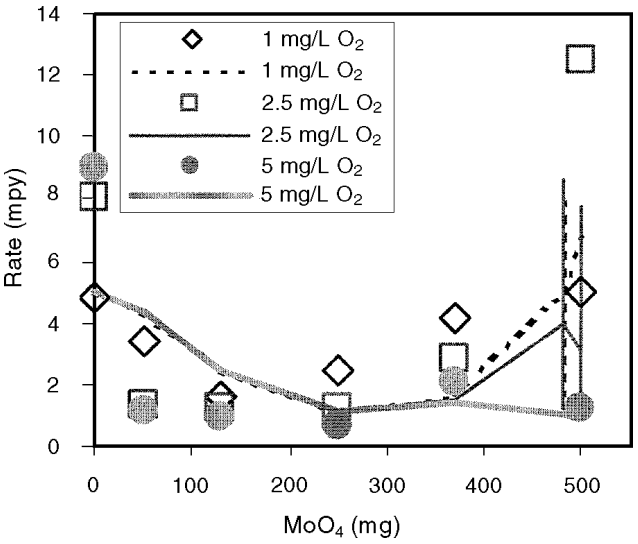

FIGURE 5. *Corrosion rates in simulated cooling water (7×10^{-3} m NaCl, 5.4×10^{-3} m Na_2SO_4, 6.25×10^{-4} $CaCO_3$, and 6.25×10^{-4} m $MgCO_3$) at 60°C inhibited with a mixture of $NaNO_2$ and N_2MoO_4 with varying composition. The total amount of dissolved inhibitor is 500 mg/L, and the amount of dissolved oxygen is 1, 2.5 ,or 5 mg/L. The lines were obtained from the model, and the symbols denote the data of Weber, et al.[40] Vertical portions of the lines denote the range between the highest and lowest rate predicted for a given composition.*

ited with only molybdate ions (i.e., for 500 mg MoO_4) depends on the concentration of dissolved oxygen. Dissolved oxygen increased the corrosion potential so that the passive range was reached. Thus, the corrosion rate in the presence of molybdate ions was reduced when the concentration of oxygen was sufficiently high. Figure 5 also illustrates the synergy between molybdate and nitrite ions for the inhibition of corrosion of carbon steel. Even with small concentrations of dissolved oxygen, the combination of nitrites and molybdates was sufficient to reduce the corrosion rate. Experimental data for this system show substantial scattering.[39] However, the predicted trends are in agreement with the data.

CONCLUSIONS

❖ A mechanistic model was developed for simulating the rates of general corrosion of selected metals in aqueous solutions. The model consists of a thermophysical module that provides comprehensive speciation calculations and an electrochemical module that predicts the partial reduction and oxidation processes on the surface of the metal. The electrochemical module is capable of reproducing the active-passive transition and the effect of solution species on passivity. The model was incorporated into a program that can be used to study the effect of conditions such as temperature, pressure, pH, solution composition, or flow velocity on corrosion rates.

❖ Model predictions were verified for a number of systems that included corrosion inhibitors. Also, the model was validated in previous papers for CO_2/H_2S corrosion and systems containing concentrated brines.[12-13] In all cases, good agreement with experimental data was obtained. Thus, the model can be used to predict corrosion rates in multicomponent systems for which experimental data are not available.

REFERENCES

1. C. de Waard, D.E. Milliams, Corrosion 31 (1975): p. 177-181.
2. C. de Waard, U. Lotz, D.E. Milliams, Corrosion 47 (1991): p. 976.
3. S. Nesic, J. Postlethwaite, S. Olsen, Corrosion 52 (1996): p. 280-294.
4. R. Zhang, M. Gopal, W.P. Jepson, "Development of a Mechanistic Model for Predicting Corrosion Rate in Multiphase Oil/Water/Gas Flows," CORROSION/97, paper no. 601 (Houston, TX: NACE International, 1997).
5. L.K. Gatzky, R.H. Hausler, "A Novel Correlation of Tubing Corrosion Rates and Gas Production Rates," in Advances in CO_2 Corrosion, eds. R.H. Hausler, H.P. Godard, vol. 1 (Houston, TX: NACE, 1984), p. 87.
6. M.R. Bonis, J.L. Crolet, "Basics of the Prediction of the Risks for CO_2 Corrosion in Oil and Gas Wells," CORROSION/89, paper no. 466 (Houston, TX: NACE, 1989).
7. J.D. Garber, F.H. Walters, R.R. Alapati, C.D. Adams, "Downhole Parameters to Predict Tubing Life and Mist Flow in Gas Condensate Wells," CORROSION/94, paper no. 25 (Houston, TX: NACE, 1994).
8. S. Srinivasan, R.D. Kane, "Prediction of Corrosivity of CO_2/H_2S Production Environments," CORROSION/96, paper no. 11 (Houston, TX: NACE, 1996).
9. A. Dugstad, L. Lunde, K. Videm, "Parametric Study of CO_2 Corrosion of Carbon Steel," CORROSION/94, paper no. 14 (Houston, TX: NACE, 1994).
10. E. Dayalan, F.D. de Moraes, J.R. Shadley, S.A. Shirazi, E.F. Rybicki, "CO_2 Corrosion Prediction in Pipe Flow Under $FeCO_3$ Scale-Forming Conditions," CORROSION/98, paper no. 51 (Houston, TX: NACE, 1998).
11. D.D. Macdonald, M. Urquidi-Macdonald, Corrosion 46 (1990): p. 380-390.

12. A. Anderko, R.D. Young, "Simulation of CO_2/H_2S Corrosion Using Thermodynamic and Electrochemical Models," CORROSION/99, paper no. 31 (Houston, TX: NACE, 1999).
13. A. Anderko, R.D. Young, "Computer Modeling of Corrosion in Absorption Cooling Cycles," CORROSION/99, paper no. 243 (Houston, TX: NACE, 1999).
14. J.F. Zemaitis, Jr., D.M. Clark, M. Rafal, N.C. Scrivner, Handbook of Aqueous Electrolyte Thermodynamics (New York, NY: AIChE, 1986), p. 852.
15. M. Rafal, J.W. Berthold, N.C. Scrivner, S.L. Grise, "Models for Electrolyte Solutions," in Models for Thermodynamic and Phase Equilibria Calculations, ed. S.I. Sandler (New York, NY: M. Dekker, 1995), p. 601-670.
16. D.M. Drazic, "Iron and Its Electrochemistry in an Active State," in Modern Aspects of Electrochemistry, eds. B.E. Conway, J.O'M. Bockris, R.E. White, no. 19 (New York, NY: Plenum Press, 1989), p. 69-192.
17. J.O'M. Bockris, D. Drazic, A.R. Despic, Electrochim. Acta 4 (1961): p. 325-361.
18. N.G. Smart, J.O'M. Bockris, Corrosion 48 (1992): p. 277-280.
19. J.M. West, Electrodeposition and Corrosion Processes (New York, NY: Van Nostrand, 1964), p. 36.
20. M. Keddam, "Anodic Dissolution," in Corrosion Mechanisms in Theory and Practice, eds. P. Marcus, J. Oudar (New York, NY: M. Dekker, 1995), p. 55-122.
21. K.J. Vetter, Electrochemical Kinetics (New York, NY: Academic Press, 1967), pp. 516, 755.
22. U. Ebersbach, K. Schwabe, K. Ritter, Electrochim. Acta 12 (1967): p. 927-938.
23. N. Sato, T. Noda, K. Kudo, Electrochim. Acta 19 (1974): p. 471-475.
24. P. Lorbeer, W.J. Lorenz, Corros. Sci. 21 (1981): p. 79.
25. P. Lorbeer, K. Juttner, W.J. Lorenz, Werkst. Korros. 34 (1983): p. 290.
26. K.E. Heusler, K.G. Weil, K.F. Bonhoeffer, Z. Physik. Chem. Neue Folge 15 (1958): p. 149.
27. K.J. Vetter, Z. Elektrochem. 59 (1955): p. 67.
28. M.A. Blesa, P.J. Morando, A.E. Regazzoni, Chemical Dissolution of Metal Oxides (Boca Raton, FL: CRC Press, 1994), p. 172.
29. K.J. Vetter, F. Gorn, Electrochim. Acta 18 (1973): p. 321.
30. K.E. Heusler, Corros. Sci. 29 (1989): p. 131.
31. J.O'M. Bockris, M.A. Genshaw, V. Brusic, H. Wroblowa, Electrochim. Acta 16 (1971): p. 1,859.
32. K.E. Heusler, B. Kusian, D. McPhail, Ber. Bunsenges. Phys. Chem. 94 (1990): p. 1,443.
33. B.D. Craig, D.S. Anderson, eds., Handbook of Corrosion Data (Materials Park, OH: ASM International, 1995), p. 1-998.
34. P.B. Mathur, T. Vasudevan, Corrosion 38 (1982): p. 171-178.
35. M.A. Stranick, Corrosion 40 (1984): p. 296-302.
36. E.A. Lizlovs, Corrosion 32 (1976): p. 263.
37. M.J. Pryor, M. Cohen, J. Electrochem. Soc. 100 (1953): p. 203-215.
38. C.M. Mustafa, S.M. Shahinoor Islam Dulal, Corrosion 52 (1996): p. 16.
39. T.R. Weber, M.A. Stranick, M.S. Vukasovich, Corrosion 42 (1986): p. 542.
40. H.C. Helgeson, D.H. Kirkham, G.C. Flowers, Amer. J. Sci. 281 (1981): p. 1,249-1,516.
41. J.C. Tanger, H.C. Helgeson, Amer. J. Sci. 288 (1988): p. 19-98.
42. E.L. Shock, H.C. Helgeson, Geochim. Cosmochim. Acta 52 (1988): p. 2,009-2,036.
43. E.L. Shock, H.C. Helgeson, Geochim. Cosmochim. Acta 54 (1990): p. 915-943.
44. D.A. Sverjensky, Rev. Mineral. 17 (1987): p. 177-209.
45. L.A. Bromley, AIChE J. 19 (1973): p. 313-320.
46. K.S. Pitzer, J. Phys. Chem. 77 (1973): p. 268-277.
47. G. Soave, Chem. Eng. Sci. 27 (1972): p. 1,197-1,203.
48. H.P. Meissner, "Thermodynamics of Aqueous Systems with Industrial Applications," S.A. Newman, ed., American Chemical Society (ACS) Symp. Ser. 133 (Washington, DC: ACS, 1980), p. 495-511.
49. V.G. Levich, Physicochemical Hydrodynamics (Englewood Cliffs, NJ: Prentice-Hall, 1962), p. 700.
50. A. Anderko, M.M. Lencka, Ind. Eng. Chem. Res. 37 (1998): p. 2,878-2,888.
51. M.M. Lencka, A. Anderko, S.J. Sanders, R.D. Young, Int. J. Thermophysics 19 (1998): p. 367-378.
52. F.P. Berger, K.-F.F.L. Hau, Int. J. Heat Mass Trans. 20 (1977): p. 1,185-1,194.
53. M. Eisenberg, C.W. Tobias, C.R. Wilke, J. Electrochem. Soc. 101 (1954): p. 306-319.

APPENDIX A—THERMODYNAMIC FRAMEWORK

In a multicomponent system, the partial molal Gibbs energy of the i-th species is related to the molality (m_i) by:

$$\overline{G}_i = \overline{G}_i^o + RT \ln m_i \gamma_i \qquad (A-1)$$

where $\overline{G}_i^0$ is the standard-state partial Gibbs energy and γ_i is the activity coefficient. Thus, the thermodynamic properties of the system can be calculated if the standard-state Gibbs energies are available for all species as functions of temperature and pressure (i.e., $\overline{G}_i^0$ [T,P]), and the activity coefficients are known as functions of the composition vector (m) and temperature (i.e., γ_i[m,T]). From basic thermodynamics, the standard-state Gibbs energy of formation $\overline{G}_i^0$ (T,P) can be calculated as a function of temperature and pressure if the following data are available:

—Gibbs energy of formation at a reference temperature and pressure (usually, T_r = 298.15 K and P_r = 1 bar);

—Enthalpy of formation at T_r and P_r;

—Entropy at T_r and P_r;

—Heat capacity as a function of temperature and pressure; and

—Volume as a function of temperature and pressure.

The key to representing the standard-state properties over substantial temperature and pressure ranges is the accurate knowledge of the heat capacity and volume. For this purpose, the Helgeson-Kirkham-Flowers-Tanger (HKFT) equation of state is used.[40-41] This equation accurately represents the standard-state thermodynamic functions for aqueous, ionic, or neutral species as functions of temperature and pressure. In its revised form,[42] the HKFT equation is capable of reproducing the standard-state properties up to 1,000°C and 5 kbar.

The HKFT equation is based on the solvation theory and expresses the standard-state thermodynamic functions as sums of structural and solvation contributions, the latter being dependent on the properties of the solvent (i.e., water). The standard partial molal volume ($\overline{V}^0$) and heat capacity ($\overline{C}_p^0$) are given by:

$$\overline{V}_0 = a_1 + \frac{a_2}{\Psi + P} + \left(a_3 + \frac{a_4}{\Psi + P}\right) \left(\frac{1}{T - \Theta}\right) - \omega Q + \left(\frac{1}{\varepsilon} - 1\right)\left(\frac{\partial \omega}{\partial P}\right)_T \qquad (A-2)$$

$$\overline{C}_p^0 = c_1 + \frac{c_2}{(T-\Theta)^2} - \left[\frac{2T}{(T-\Theta)^3}\right]\left[a_3(P-P_r) + a_4 \ln\frac{\Psi+P}{\Psi+P_r}\right] + \omega TX + 2TY\left(\frac{\partial\omega}{\partial T}\right)_p - T\left(\frac{1}{\varepsilon}-1\right)\left(\frac{\partial^2\omega}{\partial T^2}\right)_p \quad \text{(A-3)}$$

where a_1, a_2, a_3, a_4, c_1, and c_2 represent species-dependent nonsolvation parameters; T_r is the reference temperature of 298.15 K; P_r is the reference pressure of 1 bar; Ψ and Θ refer to solvent parameters equal to 2,600 bars and 228 K, respectively; and Q, X, and Y denote the Born functions given by:

$$Q = \frac{1}{\varepsilon}\left(\frac{\partial \ln\varepsilon}{\partial P}\right)_T \quad \text{(A-4)}$$

$$X = \frac{1}{\varepsilon}\left[\left(\frac{\partial^2 \ln\varepsilon}{\partial T^2}\right)_P - \left(\frac{\partial \ln\varepsilon}{\partial T}\right)_p^2\right] \quad \text{(A-5)}$$

$$Y = \frac{1}{\varepsilon}\left(\frac{\partial \ln\varepsilon}{\partial T}\right)_p \quad \text{(A-6)}$$

where ε is the dielectric constant of water and ω stands for the Born coefficient, which is defined for the j-th aqueous species by:

$$\omega_j \equiv \omega_j^{abs} - Z_j\omega_{H^+}^{abs} \quad \text{(A-7)}$$

In Equation (A-7), Z_j is the charge on the j-th aqueous species, $\omega_{H^+}^{abs}$ refers to the absolute Born coefficient of the hydrogen ion, and ω_j^{abs} designates the absolute Born coefficient of the j-th species given by:

$$\omega_j^{abs}\frac{N^0e^2Z_j^2}{2r_{e,j}} \quad \text{(A-8)}$$

where N^0 is the Avogadro number, e is the electron charge, and $r_{e,j}$ denotes the effective electrostatic radius of the j-th species, which is related to the crystallographic radius $r_{x,j}$ by:

$$r_{e,j} = r_{x,j} + |z_j|(k_z + g) \quad \text{(A-9)}$$

where k_z represents a charge-dependent constant equal to 0.0 for anions and 0.94 for cations, and g denotes a generalized function of temperature and density. Thus, the HKFT equation expresses the heat capacity and volume as functions of pure water properties and seven empirical parameters, which have been tabulated for large numbers of ions, complexes, and neutral inorganic and organic molecules. The remaining thermodynamic properties are obtained by thermodynamic integration using the values of the Gibbs energy, enthalpy, and entropy at reference temperature and pressure as integration constants.

If the HKFT equation parameters are not available from the regression of experimental data, they can be estimated. For this purpose, Shock and Helgeson presented correlations for most solution species except complexes.[42-43] Sverjensky developed an estimation method for several classes of complexes.[44] In addition to the HKFT equation parameters, these methods make it possible to predict the reference-state enthalpy and entropy if the reference-state Gibbs energy is known. These and other estimation techniques have been reviewed in detail by Rafal, et al.[15]

The activity coefficient model used for representing the solution nonideality is an extended form of an expression developed by Bromley.[45] The Bromley equation is a combination of the Debye-Hückel term for long-range electrostatic interactions and a semi-empirical expression for short-range interactions between cations and anions. In a multicomponent system, the activity coefficient of an ion i is given by:

$$\log\gamma_i = \frac{-Az_i^2I^{1/2}}{1+I^{1/2}} + \sum_j^{NO}\left(\frac{|z_i|+|z_j|}{2}\right)^2\left[\frac{(0.06+0.6B_{ij})|z_iz_j|}{\left(1+\frac{1.5}{|z_iz_j|}I\right)^2} + B_{ij} + C_{ij}I + D_{ij}I^2\right]m_j \quad \text{(A-10)}$$

where A is the Debye-Hückel coefficient that depends on temperature and solvent properties, z_i is the number of charges on ion i, I is the ionic strength (i.e., $I = 0.5\,\Sigma\, z_i^2m_i$), NO is the number of ions with charges opposite to that of ion i, and B_{ij}, C_{ij}, and D_{ij} are empirical, temperature-dependent cation-anion interaction parameters. Bromley's original formulation contains only one interaction parameter, B_{ij}, which is sufficient for systems with moderate ionic strength.[45] For concentrated systems, the two additional coefficients C_{ij} and D_{ij} usually become necessary. The three-parameter form of the Bromley model is capable of reproducing activity coefficients in solutions with ionic strength up to 30 mol/kg. The temperature dependence of the B_{ij}, C_{ij}, and D_{ij} parameters is usually expressed using a simple quadratic function.

The Bromley model is restricted to interactions between cations and anions. For ion-molecule and molecule-molecule interactions, the well-known Pitzer model is used.[46] To calculate the fugacities of components in the gas phase, the Redlich-Kwong-

Soave equation of state is used.[47] In the absence of sufficient experimental data, reasonable predictions can be made using a method proposed by Meissner,[48] which makes it possible to extrapolate the activity coefficients to higher ionic strengths based on only a single, experimental, or predicted data point.

APPENDIX B—CALCULATION OF THE MASS-TRANSFER COEFFICIENT

The mass-transfer coefficient k_m (Equations [13] and [20]) can be calculated once the flow geometry is assumed. For example, for a rotating disk, the equation of Levich holds:[49]

$$k_m = 0.62 D^{2/3} \nu^{-1/6} \omega^{1/2} \qquad \text{(B-1)}$$

where D is the diffusion coefficient of the species that undergoes the electrode reaction, ν is the kinematic viscosity, and ω is the rotation velocity. The diffusion coefficient and viscosity are calculated as functions of temperature and concentration using the methods developed by Anderko and Lencka[50] and Lencka, et al.,[51] respectively.

For straight pipe and rotating cylinder geometry, the mass-transfer coefficient can be expressed in terms of the dimensionless Reynolds (Re) and Schmidt (Sc) numbers. These numbers are defined by:

$$\mathrm{Re} = \frac{\nu d}{\nu} \qquad \text{(B-2)}$$

$$\mathrm{Sc} = \frac{\nu}{D} \qquad \text{(B-3)}$$

where ν is the linear velocity and d is the diameter. For single-phase flow in a straight pipe, the correlation of Berger and Hau can be used:[52]

$$\frac{k_m d}{D} = 0.0165\,\mathrm{Re}^{0.86}\,\mathrm{Sc}^{0.33} \qquad \text{(B-4)}$$

For a rotating cylinder, the correlation of Eisenberg, et al., applies:[53]

$$\frac{k_m d}{D} = 0.0791\,\mathrm{Re}^{0.70}\,\mathrm{Sc}^{0.356} \qquad \text{(B-5)}$$